Surface phonons and the $c(2\times2)$ oxygen overlayer on Ni(100): Theory and experiment

Talat S. Rahman
Department of Physics, Kansas State University, Manhattan, Kansas 66506

D. L. Mills
Department of Physics, University of California, Irvine, California 92717

J. E. Black
Department of Physics, Brock University, Saint Catharines, Ontario, Canada L2S 3A1

J. M. Szeftel,* S. Lehwald, and H. Ibach
Institut für Grenzflächenforschung und Vakuumphysik, Kernforschungsanlage Jülich, D-5170 Jülich, West Germany
(Received 28 November 1983; revised manuscript received 26 March 1984)

This paper presents and discusses experimental studies of surface phonons and surface-resonance modes along the line from $\bar{\Gamma}$ to $\bar{X}$ in the two-dimensional Brillouin zone, for the Ni(100) surface covered by a $c(2\times2)$ overlayer of oxygen. The data are obtained through use of off-specular electron-energy-loss spectroscopy. We also discuss data for the $p(2\times2)$ and $c(2\times2)$ overlayers, and beyond the $c(2\times2)$ overlayer where evidence of NiO formation is present. Through these spectra, the criterion for ensuring a clean $c(2\times2)$ structure is discussed. We interpret the surface-mode dispersion data for the $c(2\times2)$ overlayer successfully within the framework of a simple model which places the overlayer 0.9 Å above the surface; we cannot reconcile the data with the low-lying oxygen model discussed in earlier work. We discuss three types of lateral interactions between adsorbates, and the manner in which they influence the data: indirect interactions between adsorbates mediated by substrate atoms, direct short-ranged lateral interactions between nearest neighbors, and long-ranged dipole-dipole coupling.

I. INTRODUCTION

For many years, inelastic neutron scattering has proved a powerful and versatile means of measuring the bulk-phonon dispersion curves of crystals; of course, properties of many other elementary excitations may be studied as well. It has been recognized for some time that surface-phonon dispersion curves can provide valuable information about the properties of clean and adsorbate-covered surfaces, but until very recently experimental methods which provide both the required energy resolution and sufficient signal have been lacking.

During the past two years, two techniques have been refined to the stage where the direct measurement of surface-phonon dispersion curves is possible, for a full range of wave vectors in the two-dimensional Brillouin zone. One is inelastic atom scattering from surfaces, with neutral helium atoms used as a probe. We have data in hand for low-index surfaces of noble metals,[1,2] and for the alkali halides LiF, NaF, and KCl.[3] Also, inelastic electron scattering has provided phonon dispersion curves on the clean Ni(100) surface[4] and on Ni(100) with the $c(2\times2)$ oxygen overlayer present.[5] Here, the use of higher electron energies can lead to larger signals well off the specular direction, as suggested by theoretical analyses,[6] and at the same time one has access to the large-wave-vector transfers required to reach the boundary of the two-dimensional Brillouin zone.

In an earlier paper[5] we presented a brief account of the dispersion-curve data on the Ni(100) surface with the $c(2\times2)$ oxygen overlayer present, along with the results of theoretical calculations which provide an interpretation of the data. The present paper is devoted to a full discussion of the theoretical analysis. In addition, we include a full account of the data, including new results of studies of coverages intermediate between the $p(2\times2)$ overlayer (25% coverage) and the point where the full $c(2\times2)$ overlayer is developed (50% coverage), and extending up in coverage to the point where the presence of NiO is evidenced. Since the oxygen overlayers on Ni(100) have been the subject of much discussion in the recent literature, perhaps a summary of our principal conclusions, along with earlier viewpoints, will prove helpful at this point.

A primary issue has been the determination of the vertical distance between the outermost Ni layer and the oxygen overlayer for the $c(2\times2)$ structure. A review of the earlier history of these discussions may be found in Sec. I of the recent paper by Tong and Lau.[7] Various analyses placed the oxygen overlayer 1.5 Å above the Ni surface, 0.9 Å above it, or discovered it to be possibly coplanar. A concensus emerged which settled on the 0.9-Å vertical distance, although as Tong and Lau point out, the low-energy electron-diffraction (LEED) data admit either the 0.9-Å or nearly coplanar geometry with equal reliability.

The issue was revived recently when near-specular electron-energy-loss data (dipole-scattering regime) were obtained[8,9] on the oxygen-covered Ni(100) surface from

the $p(2\times2)$ to the $c(2\times2)$ coverage range. These spectra, which provide information on the restoring force for coherent vertical motions of the overlayer, showed that the force constant for this motion was roughly a factor of 2 lower for the $c(2\times2)$ structure than for the $p(2\times2)$ structure. At about the same time, on the basis of *ab initio* cluster calculations, Upton and Goddard[10] suggested that the oxygen was pulled down close to the Ni surface, to a point 0.27 Å above it. A theoretical analysis[11] of the dipole spectrum based on force constants provided by Upton and Goddard generated an excellent fit to the electron-energy-loss spectra, with no adjustable parameters, provided the $p(2\times2)$ overlayer resides 0.9 Å above the surface, but the $c(2\times2)$ overlayer is drawn down, as they proposed. This stimulated further experimental study of the system by other methods;[12,13] the new data suggest 0.9 Å as the vertical distance.

The present analysis, based on a full set of surface-phonon- and surface-resonance—mode dispersion curves along the line from $\bar{\Gamma}$ to $\bar{X}$ in the two-dimensional Brillouin zone, also concludes that the 0.9-Å vertical distance is the position most naturally in accord with the data. If the oxygen-Ni force constant in our nearest-neighbor central-force model is adjusted to fit the high-frequency adsorbate surface phonon (O—Ni symmetric stretching mode) at $\bar{\Gamma}$ for which the oxygen moves normal to the surface, then the frequency of the mode at $\bar{\Gamma}$ with oxygen vibrating parallel to the surface (O—Ni antisymmetric stretching mode) is fitted very well without further adjustment. With central forces only, the low-lying oxygen model produces an unphysically large value for the parallel-mode frequency, as noted earlier.[11] Introduction of angle-bending interactions reduces this frequency, through suitable adjustment of parameters, but now we find the resulting model provides a very poor account of the dispersion in the two high-frequency modes as one moves from $\bar{\Gamma}$ to $\bar{X}$. In contrast, the model with oxygen 0.9 Å above the surface provides a very nice fit when supplemented by modest lateral interactions between nearest-neighbor adsorbate atoms. Finally, the low-lying oxygen model fails to provide an adequate description of the dispersion and broadening of a resonance mode found near 200 cm^{-1}.

Very recently, Demuth and his colleagues have put forward a new model of the structure of this system.[14] On the basis of extensive new LEED data, these authors conclude that the oxygen does not sit on the fourfold site, but rather is displaced from it along the (100) direction by 0.3 Å. If the oxygen were indeed off center, the low-symmetry configuration would lead to new features in the electron-energy-loss spectrum not present if the fourfold site is occupied. For example, at $\bar{\Gamma}$ there are two high-frequency surface phonons with oxygen motion parallel to the surface. These are necessarily degenerate if the oxygen occupies the fourfold site, but they will be split if the oxygen is shifted off center. We explore the magnitude of these splittings in the theory presented below, but there is no evidence for the presence of such a lifting of the degeneracy in the data. Furthermore, if the oxygen occupies the fourfold site, selection rules require the matrix element to vanish[15] for scattering off of certain surface modes (the S_1 mode, for example) and for the scattering geometry employed in the experiments. Displacement of the oxygen off the fourfold site would lead to a breakdown in this and other selection rules which operate in our scattering geometry. We also find no evidence for such selection-rule violations. The electron-energy-loss data presented here are thus consistent with the occupancy of the fourfold site.[16]

This paper is organized as follows. In Sec. II we comment on the experimental procedures employed in these studies. New data are also presented here. The new data cover the range from the point where the $p(2\times2)$ overlayer is present until there is clear evidence of oxide formation. Then we turn to a discussion of the theoretical calculations which form the basis of our interpretation of the data. This is done in Sec. III, while in Sec. IV we summarize our principal conclusions.

II. EXPERIMENTAL DETAILS

Single crystals of nickel were cleaned by ion bombardment. Neon rather than argon was used for the bombardment because the use of neon permits the titanium-sublimation pumps to be kept at liquid-nitrogen temperatures during the sputtering, which results in a lower background pressure during the cleaning process. After sputtering, the samples were annealed to allow carbon and sulfur to segregate to the surface. Sputtering and annealing procedures were repeated until the sample was completely leached of these impurities. In the initial stages of cleansing, the impurity level was monitored with a cylindrical-mirror-analyzer— (CMA-) type Auger spectrometer. The final test for cleanness beyond the sensitivity of Auger spectroscopy was with electron-energy-loss spectroscopy, since sulfur and carbon give rise to characteristic vibrational-loss peaks when present on the surface.

The dosing of the sample with oxygen was performed by a calibrated system. The amount of oxygen to which the surface was exposed was controlled by measuring the gas pressure in a small calibrated volume using the spinning-ball friction gauge which has an absolute accuracy of 1%.[17] The samples were exposed to oxygen by opening a valve to a tube directed towards the sample with the sample positioned a few millimeters in front of the open end of the tube. An open tube rather than a microchannel plate was used because a much more uniform exposure across the sample could be achieved in this way. The ordered overlayers of oxygen were produced by exposing the clean surface at 325 K followed by a 5-min anneal to ~450 K. The LEED patterns of the $p(2\times2)$ and $c(2\times2)$ structures were used as a first check on the structures thus obtained. In the course of these and earlier experiments[8] we noticed, however, that the observation of a "sharp" LEED pattern was not sufficient evidence for a well-ordered overlayer. The final test on the structure here was again the vibration spectrum itself.

Figures 1(a) and 1(b) display spectra of well-ordered homogeneous $p(2\times2)$ and $c(2\times2)$ structures observed in near specular reflection. The two peaks in Fig. 1(a) correspond to substrate phonon losses (220 cm^{-1}) and a loss of the vertical motion of the oxygen atoms (420 cm^{-1}). The

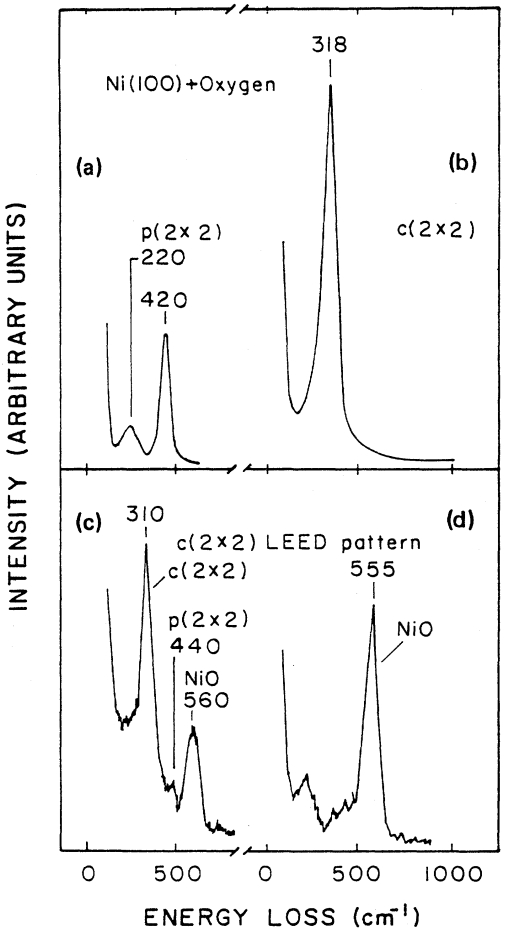

FIG. 1. Near-specular electron-energy-loss spectra taken for (a) the $p(2\times2)$ ordered oxygen overlayer on Ni(100), (b) a clean $c(2\times2)$ structure, and (c) other "$c(2\times2)$ structures" (see text) which, in fact, involve islands of both $p(2\times2)$ and NiO clusters. We also show a spectrum (d) for a surface with large amounts of NiO present. The absence of a second oxygen mode in both (a) and (b) indicates the oxygen site in the fourfold hollow site; also, the ordered structure is of high quality.

phonon loss resolves into a doublet with higher resolution.[8] For the $c(2\times2)$ structure only one oxygen mode appears in the spectrum. The spectra as displayed in Fig. 1 are unsmoothed direct-record traces.

We found that when exposures were performed at slightly higher sample temperatures with the same amount of gas, the reduced sticking coefficient would cause a somewhat lower coverage. Although the LEED pattern still remains a "sharp" $c(2\times2)$ pattern, a mixture of $p(2\times2)$ and $c(2\times2)$ islands was indicated by the presence of a small extra peak around 420 cm^{-1} (usually shifted slightly upwards) in the $c(2\times2)$ vibration spectrum.

Higher exposures than necessary to form the $c(2\times2)$ overlayer resulted in the growth of nickel oxide in the form of NiO clusters. The vibration spectrum again is a very sensitive probe to such clusters because they bear strong Fuchs-Kliewer modes[18] at 555 cm^{-1}. We found the growth of such clusters to depend on essentially three parameters: (i) exposure, (ii) sample temperature during exposure with a larger tendency towards oxide growth for *lower* temperatures, and, most importantly, (iii) the quality of the sample. Samples which were subjected to the experimental procedures too often would grow oxides more easily. We attribute this to the larger number of lattice defects on these samples which serve as nucleation centers for oxide growth. The "best" samples we had would not grow oxides when exposed to oxygen at 325 K even at very high doses, much larger doses than necessary to produce the $c(2\times2)$ vibration spectrum [as in Fig. 1(b)]. For deteriorated samples the inverse was true: Oxide clusters grew even before all islands of $p(2\times2)$ were removed. Such a spectrum is displayed in Fig. 1(c). Despite the rather messy vibration spectrum, the $c(2\times2)$ LEED pattern was very sharp. Even a side-by-side inspection of LEED photographs of the pattern associated with Figs. 1(b) and 1(c) did not reveal a significant difference, although careful LEED-intensity measurements probably would. Incidentally, even a surface which has large numbers of NiO clusters still displays a $c(2\times2)$ pattern [Fig. 1(d)].

We have attended to the issue of sample quality at length here partly because of a recent LEED investigation[14] of the $c(2\times2)$ structure where it was concluded that the oxygen assumes a position shifted by 0.3 Å sideways from the fourfold hollow site. We return to this issue later. However, in the context of the description of our experiment, it seems noteworthy to mention that according to Ref. 14 the LEED analysis was performed with a "$c(2\times2)$" structure which had an extra vibration peak near 450 cm^{-1}. We suggest that it may be worthwhile to repeat the LEED measurements on surfaces which display a vibration spectrum such as in Fig. 1(b).

This discussion then outlines our procedure for ensuring that we have a well-developed $c(2\times2)$ overlayer of oxygen, free of both a remnant of the $p(2\times2)$ structure and NiO. With samples prepared and characterized as outlined, we have carried out a sequence of off-specular energy-loss studies and have constructed dispersion curves for the various surface-phonon branches as well as a surface-resonance mode discussed below. Sample loss spectra, along with a discussion of this aspect of the experimental investigation, are given elsewhere.[5,19] We next turn to the theoretical analysis upon which our interpretation of the data is based.

III. LATTICE DYNAMICS OF THE $c(2\times2)$ OVERLAYER ON THE Ni(100) SURFACE

The $c(2\times2)$ overlayer on the (100) surface of a fcc crystal is shown in Fig. 2(a) for the case where the adsorbate is assumed to occupy the fourfold hollow site. The two-dimensional Brillouin zone for the same structure is reproduced in Fig. 2(b). The two-dimensional unit cell in this case consists of two substrate atoms (denoted by $\kappa=1$ and 2) and one adatom. The equilibrium position of each atom is specified by the vector $\vec{R}_0(\vec{l}_{||},l_z;\kappa)$, where $\vec{l}_{||}$ gives the position of the unit cell in the plane parallel to the surface, l_z labels the layer in which the atom resides, and κ denotes the different atoms inside a unit cell.

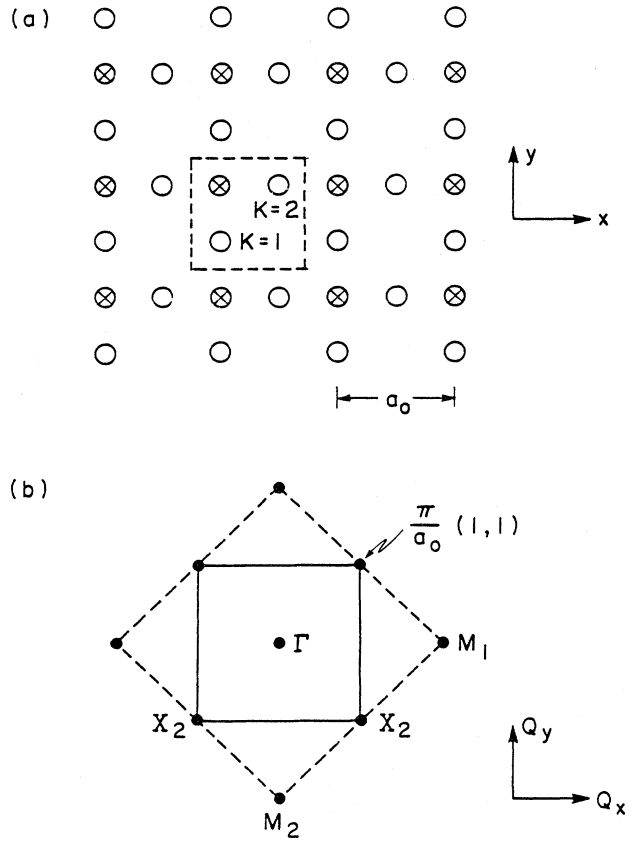

FIG. 2. (a) Illustration of the $c(2\times2)$ overlayer on the (100) surface of a fcc crystal with adsorbate atoms (marked by a cross) in the fourfold hollow site. The surface unit cell, marked by dashed lines, contains two substrate atoms in the first layer of the host atoms, with one adsorbate atom in the overlayer. (b) Two-dimensional Brillouin zone in the presence of the $c(2\times2)$ overlayer is marked with solid lines, while that for the clean (100) surface is marked by the dashed lines.

In the past[11] we have used a lattice-dynamical Hamiltonian with two-body interactions to describe the displacements of the atoms. Here, we will also include angle-bending forces (which are formally three-body interactions), which become important when the oxygen atoms occupy a low-lying position above the Ni surface. Without the angle-bending forces the frequency of vibration of the oxygen atoms parallel to the surface, for such low-lying overlayers, becomes unreasonably high.[11] The Hamiltonian is thus $H=T+V_c+V_{AB}+V_{DD}$, where T is the kinetic energy, V_c is the central-force contribution to the lattice-dynamical Hamiltonian, and V_{AB} and V_{DD} are the angle-bending and dipole-dipole terms. The latter two require a brief discussion.

First, consider the form of V_{AB}. Suppose we have atoms i and k in layer l_z, which are nearest neighbors of atom j in the layer above, such that θ is the angle between the line between i and j and that between i and k, at equilibrium. The angular displacement $\Delta\theta$ from equilibrium, to lowest order in the relative displacement $\vec{u}_{ij}$ between atom i and atom j, can then be written as

$$\Delta\theta=\frac{1}{\sin\theta}\left[\cos\theta\left[\frac{\vec{u}_{ij}\cdot\vec{R}^{\,0}_{ij}}{(R^0_{ij})^2}\right]+\frac{\vec{u}_{kj}\cdot\vec{R}^{\,0}_{kj}}{(R^0_{kj})^2}-\frac{1}{R^0_{ij}R^0_{kj}}(\vec{R}^{\,0}_{ij}\cdot\vec{u}_{kj}+\vec{R}^{\,0}_{kj}\cdot\vec{u}_{ij})\right], \tag{3.1}$$

where $\vec{R}^{\,0}_{ij}=\vec{R}_0(i)-\vec{R}_0(j)$ is the equilibrium separation between atoms i and j, and again $\vec{u}_{ij}=\vec{u}(i)-\vec{u}(j)$ is the departure from equilibrium. We have $V_{AB}=\frac{1}{2}\gamma(\Delta\theta)^2$, with γ the angle-bending force constant, and after some algebra one may write V_{AB} in the form

$$\tfrac{1}{2}\sum_l\sum_{l'}\Phi^a_{\alpha\beta}(l,l')u_\alpha(l)u_\beta(l'),$$

where the terms $\Phi^a_{\alpha\beta}(l,l')$ arising from angle-bending interactions have the following explicit forms:

$$\Phi^a_{\alpha\beta}(i,i)=\frac{\gamma}{(R^0_{ij})^2\sin^2\theta}[n_\alpha(k,j)-n_\alpha(i,j)\cos\theta]\times[n_\beta(k,j)-n_\beta(i,j)\cos\theta], \tag{3.2}$$

with a similar form for $\Phi^a_{\alpha\beta}(k,k)$, where $n_\alpha(k,j)$ is the αth Cartesian component of the unit vector from atom k to atom j, while when $i\neq k$,

$$\Phi^a_{\alpha\beta}(i,k)=\frac{\gamma}{R^0_{ij}R^0_{kj}\sin^2\theta}[n_\alpha(k,j)-n_\alpha(i,j)\cos\theta]\times[n_\beta(i,j)-n_\beta(k,j)\cos\theta]. \tag{3.3}$$

One may also readily work out the form of the remaining contributions from the expressions given above.

We now turn to the last term in the Hamiltonian, namely V_{DD}, which represents a dipole-dipole interaction between the oxygen adatoms. The vibrations of oxygen and nickel atoms (first layer) perpendicular to the surface give rise to charge fluctuations which produce dynamic dipole moments. The form of the model potential may be written in terms of the relative displacement of the oxygen and nickel atoms perpendicular to the surface. As the $c(2\times2)$ overlayer has one oxygen and two nickel atoms per unit cell, displacement of the oxygen atom relative to the nickel ones is given as follows:

$$u^s_z(\vec{l}_{||})=u_z(\vec{l}_{||},0;1)-\tfrac{1}{2}[u_z(\vec{l}_{||},1;1)+u_z(\vec{l}_{||},1;2)], \tag{3.4}$$

where the z direction is perpendicular to the crystal surface and $\vec{l}_{||}$ gives the position of the oxygen atom, i.e., $\vec{l}_{||}=a_0(n\hat{x}+m\hat{y})$, n and m being integers and a_0 the lattice constant. We assume the dynamic dipole moment associated with a given unit cell is proportional to $u^s_z(\vec{l}_{||})$; the transverse dipole moment generated by oxygen motion parallel to the surface is assumed to be cancelled by the image dipole to first approximation. Then we write V_{DD} as

$$V_{DD}=\tfrac{1}{2}(e^*)^2\sum_{\vec{l}_{||}}\sum_{\vec{l}'_{||}}{}'\frac{u^s_z(\vec{l}_{||})u^s_z(\vec{l}'_{||})}{|\vec{R}(\vec{l}_{||}-\vec{l}'_{||})^3}, \tag{3.5}$$

where e^* is the effective charge, $\vec{R}(\vec{l}_{||}-\vec{l}\,'_{||})$ is the position vector between oxygen atoms at $\vec{l}_{||}$ and that at $\vec{l}\,'_{||}$, the factor of $\frac{1}{2}$ ensures that no pair is counted twice, and the prime over the summation excludes the case $\vec{l}_{||}=\vec{l}\,'_{||}$.

We now proceed with a quick survey of our procedure for calculating the dynamic displacements of the atoms. We invoke transitional symmetry in the direction parallel to the surface to express the atomic displacements in terms of the eigenvectors $\vec{e}$, and write the displacement $u_\alpha(\vec{l}_{||},l_z;\kappa)$ associated with a given mode as

$$u_\alpha(\vec{l}_{||},l_z;\kappa)=\left[\frac{\hbar}{2M(l_z)\omega_s(\vec{Q}_{||})N_s}\right]^{1/2}e_\alpha^{(s)}(\vec{Q}_{||};l_z,\kappa)\times e^{i\vec{Q}_{||}\cdot\vec{R}_0(\vec{l}_{||},l_z;\kappa)}, \tag{3.6}$$

where s denotes a particular eigenmode associated with the wave vector $\vec{Q}_{||}$, which lies within the two-dimensional Brillouin zone of the surface with the overlayer. Then $\omega_s(\vec{Q}_{||})$ is its frequency and N_s the number of unit cells in the surface layer. As in earlier papers,[11] we construct the Green's functions for the atomic displacements from the eigenvectors below

$$U_{\alpha\beta}(l_z,\kappa;l_z',\kappa';\vec{Q}_{||},\omega)=\sum_s\frac{e_\alpha^{(s)}(\vec{Q}_{||};l_z,\kappa)e_\beta^{(s)}(\vec{Q}_{||};l_z',\kappa')}{\omega^2-\omega_s^2(\vec{Q}_{||})}, \tag{3.7}$$

where $\omega_s(\vec{Q}_{||})$ is the frequency associated with the mode s. From these, we may examine the frequency spectrum of selected atomic motions in the surface through construction of the appropriate spectral densities.

In this section we will mainly focus on the evaluation of the particular Green's functions that enter the energy-loss spectrum of the $c(2\times2)$ oxygen overlayer on the Ni(100) surface as one moves along the $\bar{\Gamma}$–$\bar{X}$ direction of the Brillouin zone, i.e., the line for which $Q_x=Q_y$.

As an example, we calculate the Green's function corresponding to the motion of oxygen atoms perpendicular to the surface, i.e., along the z axis with the x-y plane being parallel to the crystal surface. Then, with $\alpha=\beta=z$, $l_z=l_z'=0$, and $\kappa=\kappa'=1$ by proceeding as earlier,[11] we find, replacing these values of $l_z,\kappa;l_z',\kappa'$ by the short-hand symbol 0,1 for brevity,

$$\begin{aligned}&(4k_{00}r_\perp^2+\theta_1+d_{00}-\omega^2)U_{zz}(0,1;\vec{Q}_{||})\\&\quad+ir_\perp\sin(aQ_y)(2k_{01}+\theta_2)U_{||}^-(1;\vec{Q}_{||})\\&\quad-[(2k_{01}r_\perp^2+\theta_2)\cos(aQ_y)-d_{01}]U^L(1;\vec{Q}_{||})=1\ .\end{aligned} \tag{3.8}$$

Here, $r_\perp=R_\perp/a$, with $R_\perp$ the vertical height at which oxygen is taken to sit in the fourfold hollow site above the Ni(100) surface and $a=a_0/2$ and k_{00} and k_{01} are effective force constants such that, with adsorbate mass M_a, substrate mass M_s, and ϕ_{01}'', the second derivative of the pair potential between oxygen and nickel atoms can be written as follows:

$$k_{00}=\frac{\phi_{01}''}{M_a}\left[\frac{1}{1+r_\perp^2}\right],\quad k_{01}=\frac{\phi_{01}''}{(M_aM_s)^{1/2}}\left[\frac{1}{1+r_\perp^2}\right]. \tag{3.9}$$

The quantities θ_1 and θ_2 in the above equation come from angle-bending interactions between the oxygen atoms and the nearest-neighbor nickel atoms and are given by the following expressions:

$$\theta_1=\frac{8\alpha_b\phi_{01}''}{M_a(1+r_\perp^2)} \tag{3.10}$$

and

$$\theta_2=\frac{4\alpha_b\phi_{01}''}{(M_aM_s)^{1/2}(1+r_\perp^2)}, \tag{3.11}$$

where α_b is the ratio of the strength of the angle-bending interaction to the direct mechanical (spring) coupling between the atoms.

The quantities d_{00} and d_{01} arise from the dipole interactions discussed earlier and have the following forms, with $Q_x=Q_y=(\pi/a_0)\xi$:

$$d_{00}=\frac{4\pi(e^*)^2}{3a^3M_a}S(\xi), \tag{3.12}$$

$$d_{01}=-\frac{2\pi(e^*)^2}{3a^3(M_aM_s)^{1/2}}S(\xi), \tag{3.13}$$

where

$$\begin{aligned}S(\xi)=\sum_{l=1}^{\infty}\sum_{n=-\infty}^{\infty}&|n+\tfrac{1}{2}\xi|\cos(\pi l\xi)\\&\times[\pi|n+\tfrac{1}{2}\xi|K_0(2\pi l|n+\tfrac{1}{2}\xi|)\\&+l^{-1}K_1(2\pi l|n+\tfrac{1}{2}\xi|)]\ .\end{aligned} \tag{3.14}$$

The two-dimensional dipole sums have been converted to rapidly converging series, following earlier work by Benson and Mills.[20]

The functions $U_{||}^-(1;\vec{Q}_{||})$ and $U^L(1;\vec{Q}_{||})$ are combinations of Green's functions for the displacements of the first-layer nickel atoms, and are defined as follows:

$$U_{||}^-(1;\vec{Q}_{||})=U_{xz}(1,2;\vec{Q}_{||})+U_{yz}(1,1;\vec{Q}_{||}), \tag{3.15}$$

$$U^L(1;\vec{Q}_{||})=U_{zz}(1,1;\vec{Q}_{||})+U_{zz}(1,2;\vec{Q}_{||})\ . \tag{3.16}$$

The nickel atoms thus respond to vertical motion of the oxygen atoms perpendicular to the surface. Note that we have abbreviated the Green's functions $U_{\alpha\beta}(l_z,\kappa;l_z',\kappa';\vec{Q}_{||},\omega)$ to $U_{\alpha\beta}(l_z,\kappa;\vec{Q}_{||})$ in the interest of brevity. For all functions displayed, we have $l_z'=0$, $\kappa'=1$.

The displacements of the first-layer nickel atoms, in turn, couple to particular motions of the atoms in the layer above and below them, as seen in the equation for $U_{||}^-(1;\vec{Q}_{||})$,

$$\{2k'_{00}+2k_{11}[1+\sin^2(aQ_y)]+k_{12}+\theta_3 r_\perp^2[1-\cos(2aQ_y)]-\omega^2\}U_{||}^{-}(1;\vec{Q}_{||})$$
$$-2k_{01}\cos(aQ_y)U_{||}(0,1;\vec{Q}_{||})-2i(2k_{01}+\theta_2)r_\perp\sin(aQ_y)U_{zz}(0,1;\vec{Q}_{||})-2k_{11}\cos^2(aQ_y)U_{||}^{+}(1;\vec{Q}_{||})$$
$$+2ic_{12}\sin(aQ_y)U_{zz}(2,2;\vec{Q}_{||})+i\theta_3 r_\perp\sin(aQ_y)U^L(1;\vec{Q}_{||})-k_{12}\cos(aQ_y)U_{||}(2,2;\vec{Q}_{||})=0\ , \quad (3.17)$$

and also in the equation for $U^L(1;\vec{Q}_{||})$ for the displacement of the first-layer nickel atoms perpendicular to the surface,

$$\{2k'_{12}+2k'_{00}r_\perp^2+\theta_3[1+2\cos(aQ_y)]+d_{11}-\omega^2\}U^L(1;\vec{Q}_{||})-2ik_{01}r_\perp\sin(aQ_y)U_{||}(0,1;\vec{Q}_{||})$$
$$-i\theta_3 r_\perp\sin(aQ_y)U_{||}^{-}(1;\vec{Q}_{||})-2[(2k_{01}r_\perp^2+\theta_2)\cos(aQ_y)-d_{01}]U_{zz}(0,1;\vec{Q}_{||})+ic_{12}\sin(aQ_y)U_{||}(2,1;\vec{Q}_{||})$$
$$+ic_{12}\sin(aQ_y)U_{||}(2,2;\vec{Q}_{||})-2k'_{12}\cos(aQ_y)U_{zz}(2,1;\vec{Q}_{||})-2k'_{12}\cos(aQ_y)U_{zz}(2,2;\vec{Q}_{||})=0\ . \quad (3.18)$$

In the above equations the following combinations of the Green's function have been used:

$$U_{||}(0,1;\vec{Q}_{||})\equiv U_{xz}(0,1;\vec{Q}_{||})+U_{yz}(0,1;\vec{Q}_{||})\ , \quad (3.19a)$$

$$U_{||}^{+}(1;\vec{Q}_{||})\equiv U_{xz}(1,1;\vec{Q}_{||})+U_{yz}(1,2;\vec{Q}_{||})\ , \quad (3.19b)$$

$$U_{||}(2,\kappa;\vec{Q}_{||})\equiv U_{xz}(2,\kappa;\vec{Q}_{||})+U_{yz}(2,\kappa;\vec{Q}_{||})\ . \quad (3.19c)$$

The effective force constants that enter the equations are of three types: those for interaction between the oxygen and nickel atoms given by

$$k'_{00}=\frac{\phi''_{01}}{M_s}\frac{1}{1+r_\perp^2}\ , \quad (3.20)$$

those that couple the atoms within the top substrate layer defined by

$$k_{11}=\frac{\phi''_{11}}{M_s}\ , \quad (3.21)$$

where ϕ''_{11} is the corresponding potential derivative, and, finally, those that correspond to interlayer coupling between the first and second layer, with ϕ''_{12} the second derivative of the pair potential. These are given by

$$k_{12}=2\frac{\phi''_{12}}{M_s}\sin^2\theta_{12}\ , \quad (3.22)$$

$$k'_{12}=2\frac{\phi''_{12}}{M_s}\cos^2\theta_{12}\ , \quad (3.23)$$

and

$$c_{12}=2\frac{\phi''_{12}}{M_s}\sin\theta_{12}\cos\theta_{12}\ . \quad (3.24)$$

Here, θ_{12} is the angle that the unit vector between a nickel atom in the second layer and its nearest-neighbor nickel atom in the top layer makes with the z axis (perpendicular to the surface). In the absence of relaxation, θ_{12} is 45°, ϕ''_{12} attains the bulk value ϕ'', and k_{12}, k'_{12}, and c_{12} all reduce to the bulk force constant $k=\phi''/M_s$. The quantity θ_3, like θ_1 and θ_2, comes from angle-bending interactions and is defined as

$$\theta_3=\frac{2\alpha_b\theta''_{01}}{(1+r_\perp^2)M_s}\ . \quad (3.25)$$

Like the terms d_{00} and d_{01} which entered the earlier equations through dipolar interactions between the adatoms, we now have, in addition, d_{11}, which is given by

$$d_{11}=\frac{\pi(e^*)^2}{3a^3M_s}S(\xi)\ . \quad (3.26)$$

Note that, the motion of oxygen atoms parallel to the surface [$U_{||}(0,1;\vec{Q}_{||})$] appears directly in the equations for the displacements of the first-layer nickel atoms as one moves away from the $\bar{\Gamma}$ point ($\vec{Q}_{||}=\vec{0}$) of the two-dimensional Brillouin zone. The symmetric and asymmetric stretching motion of the oxygen—nickel bond are thus coupled, away from the $\bar{\Gamma}$ point. It is easy to see that these two motions are again decoupled at the high-symmetry point $\bar{X}$ of the two-dimensional Brillouin zone. In fact, at $\bar{X}$ the perpendicular motion of oxygen couples only to the parallel motion of nickel atoms and the parallel motion of oxygen only to perpendicular ones of nickel. In Fig. 3 we illustrate the pattern of motions at $\bar{X}$ for a mode in which the oxygens move parallel to the surface.

The displacement of the oxygen atoms parallel to the surface are represented by the Green's function $U_{||}(0,1;\vec{Q}_{||})$, and this, in turn, is connected to the displacement patterns of the nickel surface-layer atoms as shown in the following equation:

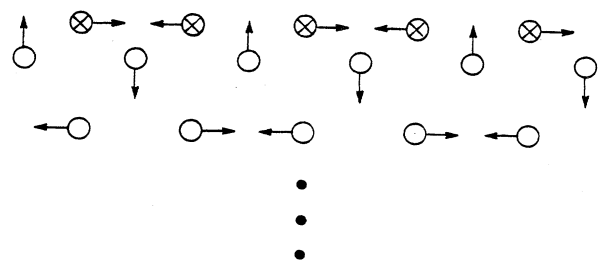

FIG. 3. Side view of motion of atoms when the parallel motion of the oxygen overlayer is excited at $\bar{X}$ in the two-dimensional Brillouin zone. At $\bar{X}$ the atomic motions associated with the S_4 surface phonon have this symmetry.

$$\{2k_{00}+2l_{00}[1-\cos(2aQ_y)-\omega^2]\}U_{||}^{-}(0,1;\vec{Q}_{||})-2k_{01}\cos(aQ_y)U_{||}^{-}(1;\vec{Q}_{||})+2ik_{01}r_{\perp}\sin(aQ_y)U^{L}(1;\vec{Q}_{||})=0\ , \tag{3.27}$$

where l_{00} is the force constant for the lateral interaction between oxygen adatoms which we write as ϕ''_{00}/M_a. Since the value of ϕ''_{00} is not known to us, l_{00} will be chosen so to fit the frequency of a certain high-frequency surface phonon at $\bar{X}$, as described below.

The Green's-function hierarchy continues to grow as we write the equations for $U_{||}^{+}(1;\vec{Q}_{||})$ and those corresponding to the displacements of the second-layer nickel atoms. Thus,

$$\{2k_{11}[1+\sin^2(aQ_y)]+k_{12}-\omega^2\}U_{||}^{+}(1;\vec{Q}_{||})-2k_{11}\cos^2(aQ_y)U_{||}^{-}(1;\vec{Q}_{||})$$
$$-k_{12}\cos(aQ_y)U_{||}(2,1;\vec{Q}_{||})+2ic_{12}\sin(aQ_y)U_{zz}(2,1;\vec{Q}_{||})=0\ , \tag{3.28}$$

while the equation of motion for $U_{zz}(2,1;\vec{Q}_{||})$, the vertical displacement of the $\kappa=1$ atom in the second nickel layer, is

$$(2k'_{12}+2k-\omega^2)U_{zz}(2,1;\vec{Q}_{||})-ic_{12}\sin(aQ_y)U_{||}^{+}(1;\vec{Q}_{||})$$
$$-k'_{12}\cos(aQ_y)U^{L}(1;\vec{Q}_{||})+ik\sin(aQ_y)U_{||}^{+}(3;\vec{Q}_{||})-k\cos(aQ_y)U^{L}(3;\vec{Q}_{||})=0\ . \tag{3.29}$$

The related equation for $U_{zz}(2,2;\vec{Q}_{||})$ is

$$(2k'_{12}+2k-\omega^2)U_{zz}(2,2;\vec{Q}_{||})-ic_{12}\sin(aQ_y)U_{||}^{-}(1;\vec{Q}_{||})$$
$$-k'_{12}\cos(aQ_y)U^{L}(1;\vec{Q}_{||})+ik\sin(aQ_y)U_{||}^{-}(3;\vec{Q}_{||})-k\cos(aQ_y)U^{L}(3;\vec{Q}_{||})=0\ , \tag{3.30}$$

and those for $U_{||}(2,1;\vec{Q}_{||})$ and $U_{||}(2,2;\vec{Q}_{||})$ are

$$(k_{12}+3k-\omega^2)U_{||}(2,1;\vec{Q}_{||})-k_{12}\cos(aQ_y)U_{||}^{+}(1;\vec{Q}_{||})-ic_{12}\sin(aQ_y)U^{L}(1;\vec{Q}_{||})$$
$$-2k\cos(2aQ_y)U_{||}(2,2;\vec{Q}_{||})-k\cos(aQ_y)U_{||}^{+}(3;Q_{||})-ik\sin(aQ_y)U^{L}(3;\vec{Q}_{||})=0 \tag{3.31}$$

and

$$(k_{12}+3k-\omega^2)U_{||}(2,2;\vec{Q}_{||})-k_{12}\cos(aQ_y)U_{||}^{-}(1;\vec{Q}_{||})-ic_{12}\sin(aQ_y)U^{L}(1;\vec{Q}_{||})$$
$$-2k\cos(aQ_y)U_{||}(2,1;\vec{Q}_{||})-k\cos(aQ_y)U_{||}^{-}(3;\vec{Q}_{||})+ik\sin(aQ_y)U^{L}(3;\vec{Q}_{||})=0\ . \tag{3.32}$$

The above nine equations, two for the displacement of oxygen atoms [Eqs. (3.8) and (3.27)], three for the displacement of first-layer nickel atoms [Eqs. (3.17), (3.18), and (3.28)], and four for the displacement of the second-layer nickel atoms, when supplemented by three equations for the displacement of third-layer nickel atoms, form a closed hierarchy considerably more complex in detail than, but similar in mathematical structure, to those described earlier.[11] We solve the hierarchy exactly by a suitable extension of our earlier procedures. Note that we have set the calculation up so the force constant between the first- and second-layer nickel atoms may differ from the bulk value. Before we can set up the solutions of the hierarchy of equations, we require those for the motions of the third and the fourth layers of nickel atoms; at this point we are deep enough in the bulk for their structure to be uninfluenced by the surface. In notation similar to that used above,

$$(4k-\omega^2)U^{L}(3;\vec{Q}_{||})-ik\sin(aQ_y)[U_{||}(2,1;\vec{Q}_{||})+U_{||}(2,2;\vec{Q}_{||})-U_{||}(4,1;\vec{Q}_{||})-U_{||}(4,2;\vec{Q}_{||})]$$
$$-2k\cos(aQ_y)[U_{zz}(2,1;\vec{Q}_{||})+U_{zz}(2,2;\vec{Q}_{||})+U_{zz}(4,1;\vec{Q}_{||})+U_{zz}(4,2;\vec{Q}_{||})]=0\ , \tag{3.33}$$

$$[4k+2k\sin^2(aQ_y)-\omega^2]U_{||}^{+}(3;\vec{Q}_{||})-k\cos(aQ_y)[U_{||}(2,1;\vec{Q}_{||})+U_{||}(4,1;\vec{Q}_{||})]$$
$$-2k\cos^2(aQ_y)U_{||}^{-}(3;\vec{Q}_{||})-2ik\sin(aQ_y)U_{zz}(2,1;\vec{Q}_{||})+2ik\sin(aQ_y)U_{zz}(4,1;\vec{Q}_{||})=0\ , \tag{3.34}$$

and, finally,

$$[4k+2k\sin^2(aQ_y)-\omega^2]U_{||}^{-}(3;\vec{Q}_{||})-k\cos(aQ_y)[U_{||}(2,2;\vec{Q}_{||})+U_{||}(4,2;\vec{Q}_{||})]$$
$$-2k\cos^2(aQ_y)U_{||}^{+}(3;\vec{Q}_{||})-2ik\sin(aQ_y)U_{zz}(2,2;\vec{Q}_{||})+2ik\sin(aQ_y)U_{zz}(4,2;\vec{Q}_{||})\ . \tag{3.35}$$

The above twelve coupled equations, supplemented by those associated with layers deep in the bulk, are solved using standard methods, as earlier, to give us the required Green's functions. We note that we then have a closed-form solution for a semi-infinite Ni(100) crystal with a $c(2\times2)$ overlayer imposed.

The equations for the bulk atoms are obtained from the equations for the second- and third-layer nickel atoms by substituting bulk values for all the effective force constants. Note that each odd-numbered layer contributes three equations and the even-numbered layer contributes four equations. These are thus seven bulk equations. We

then proceed as follows. For each of the seven functions we invoke an exponential ansatz such that

$$U^L(l_z;\vec{Q}_{||})=\sum_i f_{1i}e^{-l_z\beta_i}\ , \tag{3.36a}$$

$$U_{zz}(l_z,l;\vec{Q}_{||})=\sum_i f_{2i}e^{-l_z\beta_i}\ , \tag{3.36b}$$

etc., for the remaining members of the set. The decay constants β_i are then obtained by substituting Eqs. (3.36) into the bulk equations. For our model, we may obtain closed-form expressions for the β_i (three in number), then join the solutions of the bulk equations given in Eqs. (3.36) onto the set which describes them as vicinity of the surface.

In this section we have outlined the ingredients in the model used in our analysis of the data, and also described the method of constructing the Green's function. As in earlier work by us, the method produces an *exact* solution for the semi-infinite crystal; from the Green's function described above, we may form the spectral densities which describe, at a particular wave vector $\vec{Q}_{||}$ along the line from $\bar{\Gamma}$ to $\bar{X}$, the frequency spectrum of motions in the adsorbate layer, and also in the first nickel layers. The method for forming the spectral densities is the same as we have discussed earlier.[11] We now turn to a discussion of our results.

IV. RESULTS OF CALCULATIONS: COMPARISON WITH EXPERIMENT

We now turn to the results of our spectral-density calculations based on the formalism outlined in Sec. III. The purpose of this section is to compare the predictions of theory with experiment, and to discuss the sensitivity of various features in the phonon spectrum to the parameters which enter the theoretical model. Our philosophy is the following. We have tried to minimize the number of parameters by including only those which play a crucial role by controlling specific features in the spectrum. In the end, we find what we believe to be quite a good fit to the data with rather few parameters; we could elaborate on this basic model and improve the fit further, but before this can be done in a meaningful fashion, a larger quantity of data will be required, to ensure that the new coupling constants introduced to "fine tune" the fit along the $\bar{\Gamma}$–$\bar{X}$ line produces a phonon spectrum that is reasonable elsewhere in the two-dimensional Brillouin zone.

In Sec. I we mentioned that the suggestion[10] that the $c(2\times2)$ oxygen overlayer is pulled closer to the surface than the $p(2\times2)$ structure has been advanced in the recent literature. Our earlier work, based on data taken only at $\bar{\Gamma}$,[8] suggested that this model provides an explanation for the rather small restoring force for vertical motion found for the $c(2\times2)$ structure; the frequency of the high-frequency oxygen vibration normal to the surface drops from 440 to near 300 cm^{-1} as one moves from the $p(2\times2)$ structure to the $c(2\times2)$ structure. We find here, however, that a model which places the oxygen 0.9 Å into the $c(2\times2)$ structure [the same distance above the substrate assumed appropriate for the $p(2\times2)$ structure] provides an excellent fit to the entire phonon spectrum along the line from $\bar{\Gamma}$ to $\bar{X}$, while a more elaborate model of the low-lying oxygen overlayer fails badly. Of course, this model requires an O—Ni force constant that is smaller in value for the $c(2\times2)$ than for the $p(2\times2)$ structure. Recall that earlier we found that use of the *same* force constant for the $p(2\times2)$ and $c(2\times2)$ structures produced a substantial softening of the mode at $\bar{\Gamma}$, but this softening is insufficient to explain the data on the $c(2\times2)$ structure.

Thus, our conclusion is that the new data support the view that the $c(2\times2)$ overlayer and the $p(2\times2)$ overlayer are roughly the same distance above the surface, but the O—Ni force constant ϕ''_{01} in the high-density structure is smaller than that in the $p(2\times2)$ overlayer by a factor of 0.55. Presently, we have no clear idea why the force constant is reduced by this amount as one passes from the $c(2\times2)$. Allan[21] has stressed that one important difference between the two structures is that in the $c(2\times2)$ overlayer the oxygen always bonds to a Ni atom also bonded to a second oxygen adsorbate, while in the low-density $p(2\times2)$ structure each Ni is bonded to only one oxygen. There is thus a substantial difference in electronic structure in the two cases; it is perhaps then surprising that the O—Ni distance is very nearly the same in both cases. We note that the value of ϕ''_{10} we find for the $c(2\times2)$ structure is not anomalously small. It lies roughly halfway between the value appropriate to the linear NiO molecule and crystalline nickel oxide.

We shall begin by presenting a detailed description of our analysis of the phonon-dispersion data, under the assumption that the $c(2\times2)$ layer lies 0.9 Å above the surface. Then we turn to a brief account of our unsuccessful attempt to bring the data into accord with the low-lying oxygen model. We have also considered the effect of moving the oxygen off the fourfold site, and we conclude with a discussion of these calculations.

A. $c(2\times2)$ overlayer 0.9 Å above the surface

We begin by ignoring all angle-bending contributions to the O—Ni interactions and also the dipole-dipole interactions. We shall include the latter at a subsequent point in the discussion; they have a clear and distinct "signature" in the data as we shall appreciate. Thus, our basic model is one in which each oxygen adsorbate is coupled to its four nearest-neighbor Ni atoms via central-force interactions, and one in which we have nearest-neighbor interactions of central-force character between nearest-neighbor oxygen adsorbates, and between nearest-neighbor Ni atoms in the substrate. We may adjust the strength of the intraplanar interactions between Ni atoms in the outermost substrate layer if desired, along with the coupling between Ni atoms in the outermost substrate layer, and the second substrate layer.

We begin by focusing our attention on the frequencies of the two high-frequency surface phonons at $\bar{\Gamma}$, since the oxygen-oxygen coupling fails to influence their frequency; their frequency is also relatively insensitive to the strength of the Ni-Ni coupling in the substrate. Thus, for a start, we suppose that all Ni-Ni couplings have the same strength as realized in the bulk crystal.

Near $\bar{\Gamma}$, the mode at 310 cm^{-1} involves coherent motion of the oxygen overlayer in the vertical direction. This is the same mode which appeared in earlier near-specular studies of the $c(2\times2)$ overlayer.[9,10] If we fit this mode, we find $\phi''_{10}=9.05\times10^4$ dyn cm^2, a value smaller than that appropriate to the $p(2\times2)$ structure ($\phi''_{10}=16.29\times10^4$ dyn cm^2) by a factor of 0.55, as remarked earlier. Without further introduction of parameters, we then find 450 cm^{-1} for the frequency of the oxygen surface phonon near $\bar{\Gamma}$, for which the oxygen motion is parallel to the surface. This value is in excellent accord with the data.

At this point, it is clear that the low-lying oxygen model is in trouble. For the oxygen at 0.9 Å above the surface, the simple central-force model accounts quantitatively for a key frequency ratio at $\bar{\Gamma}$. Our earlier work[11] shows that the same model applied to the low-lying oxygen layer predicts a very large frequency (1440 cm^{-1}) for the parallel mode, with ϕ''_{10} chosen as given by Upton and Goddard (their value provides a close fit to the frequency of the perpendicular mode[11]). This is a gross disagreement between theory and experiment; we have proposed[11] that angle-bending contributions to the dynamical matrix element generated from the Ni—O—Ni bonds offer a way out of the difficulty at the expense of introducing a new parameter which adjusted to generate the correct parallel frequencies. From our earlier calculations, one sees that a very substantial angle-bending contribution is required to achieve a fit.[22] We shall return to this point later when we turn our attention to the low-lying oxygen model, but for now we return to the model which places the oxygen 0.9 Å above the surface.

With the above parameters, we may generate the dispersion curves from $\bar{\Gamma}$ to $\bar{X}$ for the two modes just described. For the scattering geometry employed in the experiments, it is the parallel mode with displacement parallel to the wave vector that is allowed to scatter the electron, according to the selection rules for nondipole scattering.[6,15] (The high-frequency surface modes have oxygen motion strictly parallel or perpendicular to the surface only at $\bar{\Gamma}$ and at $\bar{X}$. At a general point from $\bar{\Gamma}$ to $\bar{X}$ they are mixed, but we shall see they always remain predominantly perpendicular or parallel.) When the entire dispersion curve is swept out, the perpendicular mode displays the very large dispersion evident in the data. The physical origin of this dispersion is thus indirect coupling between oxygen adsorbates through the intermediary of the Ni atoms in the substrate.

The parallel polarized high-frequency surface phonon (450 cm^{-1} at $\bar{\Gamma}$) also shows substantial dispersion for this model, in contrast to the data. Its frequency decreases as one moves from $\bar{\Gamma}$, to drop 43 cm^{-1} below the experimental data at $\bar{X}$. If we add direct lateral interactions between nearest-neighbor oxygens of central-force character on physical grounds, it is clear that their role will be to stiffen the parallel mode at $\bar{X}$, while the frequency of the perpendicular mode at $\bar{X}$ is unaffected! Also, the frequency of both modes is necessarily unaffected at $\bar{\Gamma}$. Thus, we argue that this provides evidence for the presence of direct lateral interactions of short-range character between the adsorbates (we discuss the role of dipolar interactions later). We introduce this direct lateral interaction as described in Sec. III, and adjust its strength so that the parallel frequency at $\bar{X}$ is fitted. This requires us to choose the parameter l_{00} introduced in Sec. III to equal $0.1k_{00}$.

These parameters provide quite a good fit to the high-frequency surface-phonon dispersion curves, although the perpendicular mode at $\bar{X}$ lies about 13 cm^{-1} below the experimental value. We could remedy this by adding a small noncentral component to the oxygen-oxygen interaction. We have not done this because the fit we obtain is quite a good one, and it may be possible to envision other small refinements of the model with similar consequences. There can be a lack of uniqueness to conclusions reached from lattice-dynamical models applied in detail to a limited set of data, and so we prefer to concentrate on the important qualitative features in the data.

If we stop here we are left with one serious discrepancy between theory and experiment. When the $c(2\times2)$ overlayer is present in the surface, the data show that, at $\bar{X}$, the frequency of the S_4 surface phonon shifts down from the value of 135 cm^{-1} appropriate to the clean surface to the remarkably low frequency of 80 cm^{-1}. The model described in the preceding paragraphs provides the value of 122 cm^{-1} for the frequency of this mode. In our view, this suggests that there is a substantial softening of the force constants near the Ni surface when the high-density overlayer is present. Possibly, such a softening is a consequence of an outward relaxation of the outermost layer of Ni atoms when the oxygen is present. We note that Frenken *et al.*[13] have studied clean Ni(100), as well as Ni(100) covered with a $c(2\times2)$ oxygen overlayer, by means of Rutherford backscattering. The data are interpreted to suggest that, on the clean surface, there is a 3.2% *contraction* between the first and second layers, while a 5.2% *expansion* is present with the $c(2\times2)$ overlayer present. The difference in interplanar spacing, 8.4%, is substantial, and should lead to substantial changes in force constant, although a precise quantitative connection is difficult to establish for our phenomenological model.[23]

In Fig. 3 we show a side view of a slice of the crystal with the directions of the various atomic motions illustrated when the S_4 mode is excited at $\bar{X}$. In our nearest-neighbor central-force model, the frequency is independent of the coupling constant $k_{||}$ which couples two Ni atoms *within* the outermost layer of Ni atoms. Clearly, softening of the force constant between the first and second layers will lead to a decrease in the frequency of the mode. This force constant is defined as k_{12} in Sec. III, and if we alter only the value of this one force constant, we must choose $k_{12}=0.3k$ (with k being the bulk Ni—Ni force constant) to bring the S_4 mode down to 80 cm^{-1}. While more complex models may be able to fit this frequency with a less dramatic alteration of any one force constant, it is our view that so drastic a decrease in k_{12} will be a feature of any model brought into accord with the data. This softening of k_{12} has little influence on the parameters required to fit the high-frequency surface-phonon branches discussed earlier.

There is one more feature in the data which provides us

with a check on the above model. This is a peak in the data, for $\vec{Q}_{||}$ near $\bar{\Gamma}$, in the vicinity of 210 cm^{-1}. The parameters outlined above provide such a feature in the spectral density associated with *parallel* motions of the oxygen atoms. We note that a similar feature appears in earlier theoretical calculations.[11] This feature is a surface-resonance mode similar to those discussed previously,[24] except that it is associated with parallel rather than perpendicular motion of the adsorbate layer. In the data the resonance mode persists only over a portion of the line from $\bar{\Gamma}$ to $\bar{X}$; by the time one has moved 70% of the way from $\bar{\Gamma}$ to $\bar{X}$, the feature is no longer evident in the data. It behaves in a similar way in the theory. Finally, near $\bar{X}$, the theory predicts a structure near 165 cm^{-1}. There is a clear shoulder in the data in this frequency regime;[25] this is a resonance mode, again associated with parallel motions of the Ni atom (but now, near $\bar{X}$, the adsorbate layer vibrated vertically), and the frequency of this feature is, in the theory, sensitive to the interplanar force constant between Ni atoms in the outermost layer. We have not attempted an optimal fit to the data since this structure, while evident in the data, is not fully resolved. The reader shall appreciate the behavior of these resonance modes shortly, when we show the results of our spectral-density calculations.

In Fig. 4 we display the data, and the predictions of the theory are illustrated by solid lines. When we consider that our model is quite a simple one, we believe that the fit is quite good. The dashed lines show our attempt to fit the data with the low-lying oxygen model. We briefly discuss these calculations below. Figure 4 is the same as that presented in Ref. 5, incidentally. We reproduce the figure here for completeness. We note that once the parameters are chosen via the fitting procedure described above, they are "fine tuned" slightly in order to obtain the best overall fit, judged simply by the eye.

In Fig. 4 dipole-dipole interactions are ignored. In fact, if one examines the behavior of the high-frequency surface phonon produced by perpendicular motion of the oxygen overlayer, in the near vicinity of $\bar{\Gamma}$, there is a very clear and distinct upturn in frequency, as one moves in toward $\bar{\Gamma}$. This is, in fact, produced by the dipole-dipole interactions between the vibrating oxygen atoms. In Fig. 5 we show new dispersion curves calculated with the inclusion of dipole-dipole interactions, treated as described in Sec. III. The dynamic effective charge parameter e^* has been chosen equal to $0.4e$, a value also consistent with a rough estimate of the intensity of the 320-cm^{-1} feature very near the specular direction, where dipole scattering dominates [see, for example, Fig. 2(a) of Ref. 5]. We see a clear upturn in the theory near $\bar{\Gamma}$, very similar to that present in the data. We note that Anderson and Persson[26] have studied the dispersion of the CO stretching vibration near $\bar{\Gamma}$ in order to find similar behavior produced by dipole-dipole coupling within the CO overlayer. The data here, which extend all the way from $\bar{\Gamma}$ to $\bar{X}$, show that the dipolar interactions introduce a clear structure in the dispersion curves, one distinct from that produced by short-ranged lateral interactions. The absence of such behavior in the parallel mode is consistent with the notion that parallel dipole moments are screened strongly by the substrate; a selection rule[6,15] requires that the intensity of the parallel mode vanishes as $\bar{\Gamma}$ is approached, so it is, in fact, impossible to follow this feature all the way to $\bar{\Gamma}$.

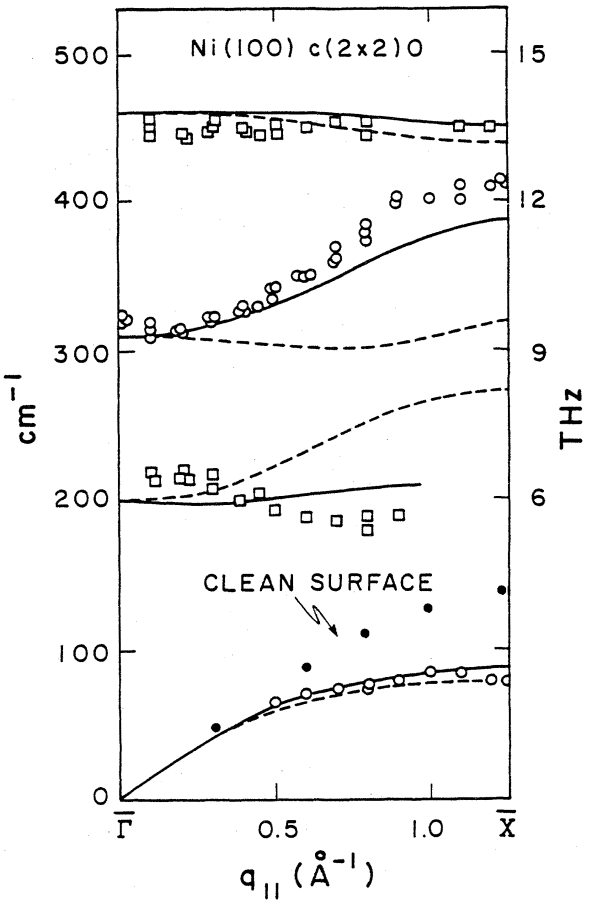

FIG. 4. Fit between the data, the model which places the oxygen overlayer 0.9 Å above the surface (solid lines), and that which places it 0.26 Å above the surface (dashed lines). For the case where the oxygen is 0.9 Å above the surface, the following parameters are used (see Sec. III): $\phi''=3.79\times10^4$ dyn/cm, $\phi''_{10}=9.5\times10^4$ dyn/cm, $k_{12}=0.3k$, and $l_{00}=0.1k_{00}$. No dipole-dipole interactions are incorporated at this point. For the low-lying oxygen model, the angle-bending parameter α_b has been chosen to be equal to 0.12. Solid circles show the dispersion relation measured for the S_4 mode on the clean surface.

The conclusions outlined above follow from study of the spectral-density functions constructed from the Green's functions described in Sec. III; the spectral densities are formed as in earlier work and provide a physical picture of the atomic motions associated with the various features. We next turn to a discussion of the structures present in these spectral-density functions. The information is summarized in Figs. 6–10. Each figure presents four spectral-density functions, each of which describes the frequency spectrum of the contribution of a particular atomic motion to the displacements from equilibrium associated with a particular wave vector along the line from $\bar{\Gamma}$ to $\bar{X}$. Along this line, we have $Q_x=Q_y=(\pi/a_0)\xi$, where ξ ranges from 0 to 1. Part (a) of each figure describes the frequency spectrum of oxygen vibrations asso-

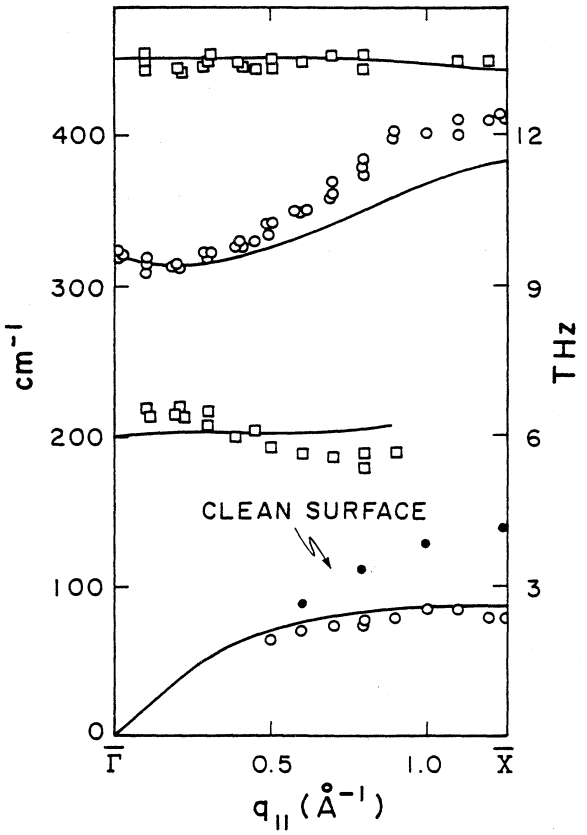

FIG. 5. Calculations of the dispersion relations of the various features in the energy-loss spectrum, with inclusion of dipole-dipole interactions modeled as described in Sec. III. We have chosen $e^*=0.4e$, and other parameters have been slightly altered from those employed in Fig. 4. Thus, $\phi''=3.74\times10^4$ dyn/cm (as before), $\phi''_{10}=9.25\times10^4$ dyn/cm, $k_{12}=0.3k$ (as before), and $l_{00}=0.1k_{00}$.

ciated with the value of ξ indicated on the figure, while each part (b) describes motions of the Ni atoms in the first substrate layer. In all cases, the solid line gives the frequency spectrum of motions normal to the surface, while the dashed line gives that of motions parallel to the surface (and also parallel to the line from $\bar{\Gamma}$ to $\bar{X}$).

Figure 6 describes $\xi=0.1$, a wave vector very close to $\bar{\Gamma}$. We see the two high-frequency surface phonons near $\bar{\Gamma}$, one near 300 cm^{-1} and one at 450 cm^{-1}. Each of these modes involves principally motion of the oxygen adlayer. Strictly speaking, such true surface modes generate Dirac δ functions in the spectral densities. These have been broadened out artificially, as earlier. Note that all spectral-density functions displayed here are formed from Green's functions as defined in Eq. (3.10). If the contribution of a given peak to the actual physical mean-square displacement is to be assessed, then the oxygen spectral densities should be multiplied by $(1/M_O)$, with M_O the mass of an oxygen atom, while the Ni spectral densities should be multiplied by $(1/M_{Ni})$. Also evident in Fig. 6 is the resonance mode near 200 cm^{-1}. As remarked earlier, this is a structure embedded within the bulk-phonon bands of the substrate, so while it generates a very clear

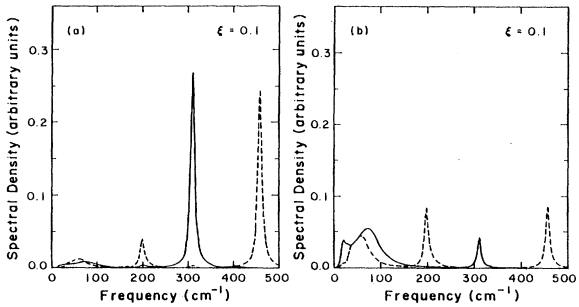

FIG. 6. Spectral-density functions, calculated from the Green's functions in Eq. (3.10), for (a) perpendicular and parallel motion of the atoms in the oxygen adlayer (solid and dashed lines, respectively), and (b) perpendicular and parallel motions of atoms in the first Ni layer (solid and dashed lines, respectively). The calculations are for $\xi=0.1$, where along the line from $\bar{\Gamma}$ to $\bar{X}$, $Q_x=Q_y=(\pi/a_0)\xi$.

and distinct peak in the spectral density, the peak does not describe an eigenmode of the system, but instead describes a resonance of the surface region, with finite lifetime in the harmonic approximation. Properties of such resonance modes have been discussed earlier.[11,24] We see from the figure that the resonance mode is here a roughly equal admixture of oxygen and nickel motion, each parallel to the surface (recall the earlier remark about the relation of these plots to the contribution of a feature to the actual mean-square displacement).

In Fig. 7 we move to $\xi=0.3$. Clearly, the two high-frequency surface phonons now each contain an admixture of motion parallel and perpendicular to the surface, although each remains quite close in character to the polarization at $\bar{\Gamma}$. The S_4 mode appears as a prominent peak near 50 cm^{-1} in the Ni spectral density for motion normal to the surface, and in this portion of the Brillouin zone, the oxygen atoms are only weakly excited into a motion parallel to the surface. The feature near 100 cm^{-1} is also a surface-resonance mode that will show appreciable dispersion to persist all the way to $\bar{X}$. This resonance mode is not evident in the data this close to $\bar{X}$, although there is clear evidence for its presence in the loss spectrum associated with larger values of $\vec{Q}_{||}$. As we move out into the zone, the 200-cm^{-1} feature weakens in intensity, while the low-frequency resonance mode in the Ni parallel spectral density increases in strength, and moves to higher frequencies. This is evident in Fig. 8 for $\xi=0.5$.

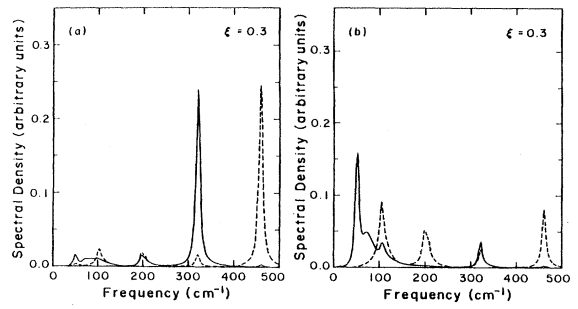

FIG. 7. Same as Fig. 6, except $\xi=0.3$.

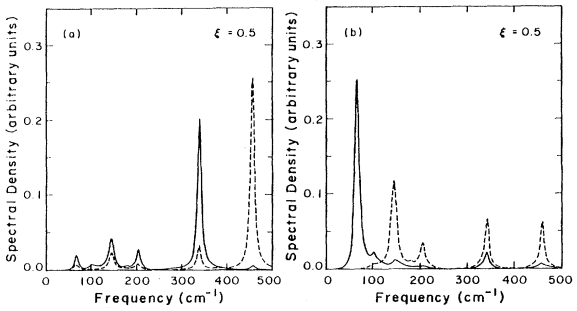

FIG. 8. Same as Fig. 6, except $\xi=0.5$.

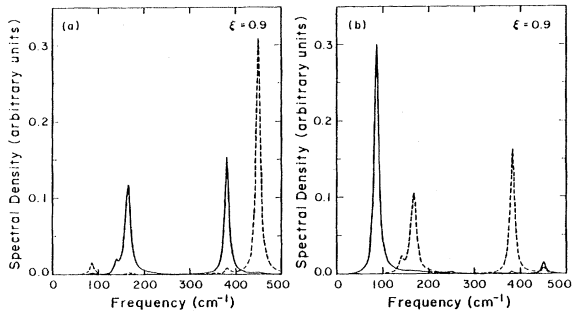

FIG. 10. Same as Fig. 6, except $\xi=0.9$.

By the time $\xi=0.7$ (Fig. 9), the feature near 200 cm^{-1} is very weak and it has indeed vanished from the data as well. We now have a prominent structure near 160 cm^{-1}; this feature, the resonance mode mentioned earlier, is associated with perpendicular motions of the oxygen atoms, and parallel motions of the Ni atoms in the first substrate layer. There is clear evidence for a feature in the data in this spectral regime as we have seen, although it does not appear as a fully resolved loss peak. For example, if one examines Fig. 2(c) of Ref. 7, which corresponds to a value of ξ not far from 0.7, there is a clearly defined shoulder which emerges from the shoulder of 75-cm^{-1} loss peak (the S_4 mode) and extends to 190 cm^{-1}, but it is unfortunately not resolved.

Finally, Fig. 10 shows the spectral densities at $\xi=0.9$. The resonance mode in the 165-cm^{-1} region remains strong in the theory, and the shoulder discussed in the preceding paragraph remains evident in the data taken at $\bar{X}$ [Fig. 2(d) of Ref. 5]. Since this resonance mode has motion of the first-Ni-layer atoms parallel to the surface associated with it, its frequency will be sensitive to the intraplanar Ni force constants, within the first layer, as remarked earlier.

This completes our discussion of the $c(2\times2)$ overlayer of oxygen on Ni(100) when the layer is assumed to lie 0.9 Å above the Ni substrate. We obtain quite a good fit to all features of the data within a rather simple model. Indeed, each prominent structure in our spectral-density functions clearly appears in the data. At the time of this writing we cannot make meaningful statements about the relative intensities of the various features. Our spectral-density functions, weighted by suitable prefactors, provide a measure of the contribution of a given feature to the mean-square displacement of the relevant atoms. However, the electron-energy-loss spectrum is given by this mean-square displacement, multiplied by a matrix element which must be calculated by a rather complex microscopic theory,[6] for experiments such as this where off-specular losses are studied. It is clear from the expected densities displayed above that *both* oxygen and Ni atoms contribute to the inelastic scattering amplitude. Throughout the zone, the high-frequency surface phonons primarily involve motion of the oxygen atoms, while the S_4 mode has its largest amplitude in the first Ni layer, as one sees from Fig. 10, for example. Under these circumstances, one can say rather little about the relative intensities of the various features in the absence of a full microscopic calculation. Such studies are underway for this system and will be reported elsewhere.

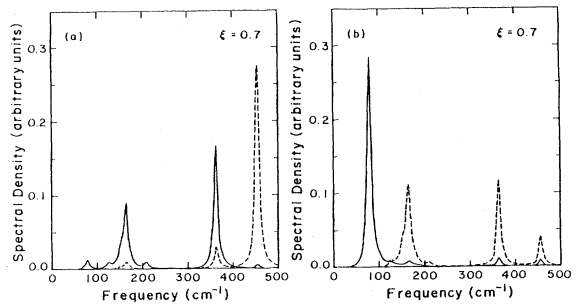

FIG. 9. Same as Fig. 6, except $\xi=0.7$.

We summarize the discussion just presented by noting that the data provide direct evidence for lateral interactions between adsorbates with three distinctly different physical origins. These are the following.

(i) Indirect interactions between oxygen adsorbates via the substrate motions: We have seen that the very large dispersion of the high-frequency surface phonon with oxygen motion is dominated by lateral interactions of this type. The short-ranged interactions of central-force character included in our model leave the frequency of this mode at $\bar{\Gamma}$ (320 cm^{-1}) and also the frequency at $\bar{X}$ unaffected, and so the very large dispersion evident in the theory and in the data has its origin in indirect interactions via the motion of substrate atoms. Such interactions will play a minor role in the $p(2\times2)$ structure, since, as discussed earlier,[15] such couplings are most pronounced when two oxygens share a common bond to the same atom in the first substrate layer.

(ii) Direct, short-ranged lateral interactions between oxygen adsorbates: In our analysis of the high-frequency surface phonon with oxygen motion parallel to the surface, such interactions are required to explain the very flat character of the dispersion curve. In essence, in our analysis, such couplings stiffen the response of the adsorbate layer progressively as one moves from $\bar{\Gamma}$ to $\bar{X}$, to act in opposition to the indirect interactions through the substrate [item (i) above], which produces *negative* dispersion in the high-frequency parallel polarized mode.

(iii) Long-ranged dipole-dipole interactions: As discussed above, these produce an upturn in the dispersion relation of the high-frequency perpendicularly polarized surface phonon as one moves toward $\bar{\Gamma}$ from $\bar{X}$. The behavior we find is very similar to that observed earlier[26]

in electron-energy-loss studies of the dispersion of the C—O stretching vibration.

As remarked in Sec. I, one may inquire if the low-lying oxygen layer can provide a fit to the data. Next, we turn to a brief account of our attempts to account for the data with this model.

B. $c(2\times2)$ overlayer 0.26 Å above the surface

Next, we describe our attempts to fit the data with the oxygen layer drawn close to the surface, as discussed in earlier papers.[10,11]

If we begin by placing the oxygen in this position, then choose ϕ''_{10} to fit the frequency of the perpendicular mode at $\bar{\Gamma}$, as noted earlier, the parallel-mode frequency at $\bar{\Gamma}$ is far higher than observed. As suggested before,[11] the addition of angle-bending terms in the potential energy provide a means of softening ϕ''_{10} and thus lowering the parallel-mode frequency at $\bar{\Gamma}$, while the perpendicular-mode frequency is left relatively unaffected. It is clear on physical grounds that the angle-bending terms "stiffen" the perpendicular response substantially and affect the parallel mode.

If we accept this means of fitting the mode at $\bar{\Gamma}$, then use the model to sweep out the dispersion curves from $\bar{\Gamma}$ to $\bar{X}$, the results differ very substantially from the data. The results are given as dashed lines in Fig. 4. There is surprisingly little dispersion in the perpendicular branch; as we have seen, nearest-neighbor central-force interactions between adsorbates leave the perpendicular-mode frequency at $\bar{X}$ unaffected, so the discrepancy cannot be resolved in this fashion. A very substantial modification of the basic force-constant model will be required to bring the theory into accord with the data; we have not examined this question further, since the very straightforward and simple picture discussed in the preceding subsection allows us to come quite close to fitting the data, as we have seen. Note also that the low-lying oxygen model leads to very substantial dispersion in the 210-cm^{-1} resonance mode at $\bar{\Gamma}$, and that this feature now persists all the way from $\bar{\Gamma}$ to $\bar{X}$ in the theory.

The earlier suggestion that the oxygen was pulled close to the surface was based, in essence, on a single data point in Fig. 4. It is not possible to bring this picture into accord with the full set of data displayed in the figure, as far as we can see.

C. Oxygen displaced off the fourfold site

As remarked in Sec. I, a recent LEED study[14] has led to the proposal that the oxygen does not, in fact, occupy the fourfold hollow site, as assumed in the analyses presented above, but is instead displaced off the fourfold site by 0.3 Å in the (100) direction. If such a displacement is indeed present, in principle there are several ways in which the electron-energy-loss spectrum would be influenced. For example, the two parallel polarized high-frequency surface phonons would no longer be degenerate as they are when the oxygen resides in the fourfold site, but they would be split. Furthermore, there will be a breakdown of the selection rule which forbids the scattering from the parallel mode polarized normal to the line from $\bar{\Gamma}$ to $\bar{X}$, so the feature near 450 cm^{-1} will appear as a doublet. Also, the breakdown of symmetry means that, even at high-symmetry points of the Brillouin zone, the normal modes will have mixed character, consisting of motions perpendicular as well as parallel to the surface. Thus, the parallel modes near 450 cm^{-1} will become dipole active near $\bar{\Gamma}$, and one will see a dramatic increase in intensity associated with dipole scattering as one approaches $\bar{\Gamma}$ from $\bar{X}$.

In the data we see no evidence for features in the energy-loss spectrum such as those described above, and thus the data are consistent with occupancy of the high-symmetry fourfold site. Of course, one must inquire if the proposed displacement off the fourfold site, 0.3 Å, will actually produce splittings or selection-rule violations sufficiently large to be resolved in the experimental spectra. To explore this question, we have carried out studies of the dispersion relations of the high-frequency surface-phonon branches, and their polarization properties, along the line from $\bar{\Gamma}$ to $\bar{X}$, for a model of the $c(2\times2)$ oxygen overlayer 0.9 Å above the surface, but displaced 0.3Å along the (100) direction. The periodic cluster method described by one of us[27] was employed. The results are summarized in Table I.

In the table, the ratio F is the ratio of the force constant associated with the short O—Ni bond to that associated with the long bonds (the term force constant here refers to the value of ϕ'', the second derivative of the appropriate pair potential). Since we have no *a priori* means of estimating this ratio, we have explored various properties as a function of F, with F varied from 1 to 5.

The first two rows in Table I describe calculations for undisplaced oxygen; the column labeled D indicates the horizontal displacement off the oxygen off the fourfold site. The two first rows in the table provide an indication of the accuracy of the periodic cluster method. The first row, for our choice of parameters, are the frequencies at $\bar{\Gamma}$ and $\bar{X}$ provided by the Green's-function method, which constitutes an exact solution of our model of the semi-infinite nickel crystal with a $c(2\times2)$ overlayer. The second row gives the frequencies provided by the periodic cluster method, which is an approximation scheme. The frequencies provided by this approximate scheme are in error from 1% to 3%, but, of course, the degeneracies are given properly.

The last four rows of Table I give the frequencies of the various modes as the oxygen is displaced by 0.3 Å for various values of F. Even when $F=1$, the fact that bond angles change as the oxygen is displaced alters the dynamical matrix $d_{\alpha\beta}(\vec{l}_{||},l_z,\kappa;\vec{l}'_{||},l'_z,\kappa')$ [see, for example, Eq. (4.15) of Ref. 15. In the present calculation, the terms in ϕ' are ignored since they are typically small in magnitude], and the calculated frequencies are thus influenced by the displacement off the high-symmetry site.

In Table I the modes are labeled $\nu_\perp$, $\nu_{||}^{(1)}$, and $\nu_{||}^{(2)}$ even though, as discussed above, the modes are no longer polarized strictly parallel or perpendicular to the surface with the oxygen off center. The mode $\nu_\perp$ is the mode which at $\bar{\Gamma}$ is strictly normal to the surface with the oxygen in the fourfold site, $\nu_{||}^{(1)}$ is the frequency of the parallel mode po-

TABLE I. Results of the study of surface-phonon frequencies and eigenvectors with oxygen displaced off the fourfold site in the (100) direction by the distance D. We have F, the ratio of the force constant associated with the short O—Ni bond to that of the long bond, and we write $Q_x=Q_y=(\pi/a_0)\xi$. The subscripts on the various modes refer to the polarization of the oxygen motion at $\bar{\Gamma}$, with $D=0$. Then (for $D=0$), $\nu_{\parallel}^{(1)}$ is the mode with displacement parallel to the surface and normal to the line from $\bar{\Gamma}$ to $\bar{X}$ while $\nu_{\parallel}^{(2)}$ is the parallel mode with displacement parallel to the line from $\bar{\Gamma}$ to $\bar{X}$. Finally, R is the ratio of the normal to the parallel component of displacement for the mode $\nu_{\parallel}^{(2)}$, when the oxygen is displaced as indicated.

			$\bar{\Gamma}$				$\bar{X}$
F	D (Å)	ξ	0.0	0.1	0.2	0.5	1.0
1.0	0.0	$\nu_{\perp}$	310	312	316	338	387
		$\nu_{\parallel}^{(1)}$	458	458	456	445	414
		$\nu_{\parallel}^{(2)}$	458	458	456	445	414
		R					
1.0	0.0	$\nu_{\perp}$	301	302	306	330	377
		$\nu_{\parallel}^{(1)}$	456	455	453	435	412
		$\nu_{\parallel}^{(2)}$	456	456	454	442	412
		R	0.000	0.036	0.072	0.174	0.000
1.0	0.3	$\nu_{\perp}$	301	303	306	327	366
		$\nu_{\parallel}^{(1)}$	451	450	447	431	410
		$\nu_{\parallel}^{(2)}$	445	445	443	433	410
		R	0.027	0.047	0.082	0.195	0.268
1.5	0.3	$\nu_{\perp}$	301	302	306	327	367
		$\nu_{\parallel}^{(1)}$	464	462	460	446	427
		$\nu_{\parallel}^{(2)}$	447	446	445	435	410
		R	0.250	0.254	0.268	0.350	0.519
2.0	0.3	$\nu_{\perp}$	301	302	306	325	355
		$\nu_{\parallel}^{(1)}$	493	492	490	477	460
		$\nu_{\parallel}^{(2)}$	475	474	473	465	450
		R	0.430	0.434	0.446	0.530	0.714
5.0	0.3	$\nu_{\perp}$	301	301	304	319	339
		$\nu_{\parallel}^{(1)}$	677	677	675	666	655
		$\nu_{\parallel}^{(2)}$	671	671	671	667	663
		R	0.754	0.756	0.763	0.804	0.866

larized normal to the $\bar{\Gamma}$–$\bar{X}$ line for this case (this is a pure parallel mode all the way from $\bar{\Gamma}$ to $\bar{X}$), while $\nu_{\parallel}^{(2)}$ is the frequency of the parallel mode with displacement parallel to the $\bar{\Gamma}$–$\bar{X}$ line when the oxygen is on the fourfold site.

In the calculations the force-constant ratio has been adjusted to provide the value of F indicated, and their absolute values are then adjusted so $\nu_{\perp}$ always equals 301 cm^{-1} at $\bar{\Gamma}$. The calculated splittings are remarkably small, even for the largest value of F considered. These splittings are small compared to the resolution of the experiment and could not have been resolved.

The factor R displayed in the table is the ratio of the normal component of displacement associated with the mode $\nu_{\parallel}^{(2)}$ to the component parallel to the surface and also to the line from $\bar{\Gamma}$ to $\bar{X}$. Near $\bar{\Gamma}$, even for modest values of the force-constant ratio F, the ratio R is remarkably large. For $F=2$, a value we suspect to be smaller than the force-constant change associated with such a large displacement off the fourfold site, we have $R=0.43$ at $\bar{\Gamma}$. The parallel mode should thus become dipole active near $\bar{\Gamma}$ as a consequence of its mixed character; if we assume the dynamic effective charge $e^*=0.4e$ used earlier in this section, the dipole activity induced by the shift of the oxygen off the fourfold site should be evident in the data. Figure 1(a) of Ref. 5 shows no evidence for a dipole signal from the high-frequency parallel mode; the electron-energy-loss data thus suggest that it is the fourfold site which is occupied. From Sec. II, we see that it is possible to prepare samples which show a sharp $c(2\times2)$ LEED pattern and also produce a feature in the dipole

near 450 cm^{-1}. However, as we argue there, such spectra are associated with surfaces which contain islands of the $p(2\times2)$ structure co-existing with the $c(2\times2)$ overlayer, and there is no evidence of a feature in this frequency regime in the near-specular electron-energy-loss spectrum taken on the samples employed in the present work.

ACKNOWLEDGMENTS

One of us (J.M.S.) wishes to thank the Alexander von Humboldt Foundation for support. This work has also been supported by the U.S. Department of Energy through Contract No. DE-AT0379-ER10432.

*Permanent address: Service de Physique des Atomes et des Surfaces, Centre d'Etudes Nucléaires de Saclay, Institut de Recherche Fondamentale, Commissariat à l'Energie Atomique, F-91191 Gif-sur-Yvette, France.

[1]G. J. M. Horne and D. R. Miller, Phys. Rev. Lett. **41**, 511 (1978); M. Cates and D. R. Miller, J. Electron Spectrosc. Relat. Phenom. **30**, 157 (1983); Phys. Rev. B **28**, 3615 (1983).

[2]R. B. Doak, U. Harten, and J. P. Toennies, Phys. Rev. Lett. **51**, 578 (1983).

[3]G. Brusdeylins, R. B. Doak, and J. P. Toennies, Phys. Rev. Lett. **46**, 437 (1981); Phys. Rev. B **27**, 3662 (1983).

[4]S. Lehwald, J. Szeftel, H. Ibach, T. S. Rahman, and D. L. Mills, Phys. Rev. Lett. **50**, 518 (1983).

[5]J. Szeftel, S. Lehwald, H. Ibach, T. S. Rahman, J. E. Black, and D. L. Mills, Phys. Rev. Lett. **51**, 268 (1983).

[6]S. Y. Tong, C. H. Li, and D. L. Mills, Phys. Rev. Lett. **44**, 407 (1980); C. H. Li, S. Y. Tong, and D. L. Mills, Phys. Rev. B **21**, 3057 (1980).

[7]S. Y. Tong and K. H. Lau, Phys. Rev. B **25**, 7382 (1982).

[8]S. Lehwald and H. Ibach, in *Vibrations at Surfaces,* edited by R. Caudano, J. M. Gilles, and A. A. Lucas (Plenum, New York, 1982), p. 137.

[9]S. Andersson, Surf. Sci. **79**, 385 (1979).

[10]T. Upton and W. A. Goddard, Phys. Rev. Lett. **46**, 1635 (1981).

[11]T. S. Rahman, J. E. Black, and D. L. Mills, Phys. Rev. Lett. **46**, 1569 (1981); Phys. Rev. B **25**, 883 (1982).

[12]J. Stöhr, R. Jaeger, and T. Kendelewicz, Phys. Rev. Lett. **49**, 142 (1982).

[13]J. W. M. Frenken, J. F. van der Veen, and G. Allan, Phys. Rev. Lett. **51**, 1876 (1983).

[14]J. E. Demuth, N. J. DiNardo, and G. S. Cargill, Phys. Rev. Lett. **50**, 1373 (1983).

[15]See H. Ibach and D. L. Mills, *Electron Energy Loss Spectroscopy and Surface Vibrations* (Academic, New York, 1982), Chap. 5.

[16]This conclusion is also consistent with more recent LEED data by H. Richter and U. Gerhardt [Phys. Rev. Lett. **51**, 1570 (1983)].

[17]G. Comsa, J. K. Fremery, B. Linderau, G. Messer, and R. Röhl, J. Vac. Sci. Technol. **17**, 642 (1980).

[18]G. Dalmai-Imelik, J. C. Bertolini, and J. Rousseau, Surf. Sci. **63**, 67 (1977).

[19]H. Ibach, in Proceedings of the Vth International Conference on Solid Surfaces (Madrid, 1983) (unpublished).

[20]H. Benson and D. L. Mills, Phys. Rev. **178**, 836 (1969).

[21]G. Allan (private communication).

[22]See Table I of the Phys. Rev. B paper cited in Ref. 11.

[23]An empirical model which connects the lattice relaxation to changes in force constant has been described in Ref. 13. The conclusions of these authors are qualitatively similar to ours.

[24]Talat S. Rahman, J. E. Black, and D. L. Mills, Phys. Rev. B **27**, 4059 (1983).

[25]See, for example, Figs. 2(c) and 2(d) of Ref. 5.

[26]S. Andersson and B. N. J. Persson, Phys. Rev. Lett. **45**, 1421 (1980).

[27]J. E. Black, Surf. Sci. **116**, 240 (1982).